Letter | Editors' Suggestion

Weak ferromagnetism in $Tb(Fe_{0.2}Mn_{0.2}Co_{0.2}Cr_{0.2}Ni_{0.2})O_3$ high-entropy oxide perovskite thin films

Alan Farhan,[1,*] Federico Stramaglia,[2] Maria Cocconcelli,[1,3] Nikolai Kuznetsov,[1] Lide Yao,[4] Armin Kleibert,[2] Cinthia Piamonteze,[2] and Sebastiaan van Dijken[1]

[1]*Department of Applied Physics, Aalto University School of Science, P.O. Box 15100, FI-00076 Aalto, Finland*
[2]*Paul Scherrer Institute, Forschungsstrasse 111, 5232 Villigen PSI, Switzerland*
[3]*Dipartimento di Fisica, Politecnico di Milano, 20133 Milano, Italy*
[4]*Nanomicroscopy Center, Aalto University School of Science, P.O. Box 15100, FI-00076 Aalto, Finland*

(Received 10 June 2022; revised 25 July 2022; accepted 29 July 2022; published 16 August 2022)

We have studied the structural and magnetic properties of $Tb(Fe_{0.2}Mn_{0.2}Co_{0.2}Cr_{0.2}Ni_{0.2})O_3$ (T5BO) high-entropy oxide perovskite (HEOP) thin films. Using synchrotron-based x-ray absorption spectroscopy, employing x-ray magnetic circular dichroism, we performed an element-sensitive study of epitaxial T5BO thin films. The measurements reveal a magnetic multiphase with variable ferromagnetic ordering of all transition metal elements, providing a promising route towards designer ferroic properties in Tb-based HEOP thin films.

DOI: 10.1103/PhysRevB.106.L060404

Rare-earth transition metal oxide perovskites with the general formula ABO_3 (A: rare-earth ion; B: 3d transition metal ions) have been the focal point of intense research efforts in recent decades due to a wide range of ferroic properties and functionalities [1,2]. The magnetic interaction between the rare-earth ions and the 3d transition metal ions has been found to be a key ingredient in determining a variety of properties such as magnetocaloric, magnetoelectric, and multiferroic behavior [3–5]. Within this group, Tb-based transition metal perovskites represent an interesting collection of compounds with diverse properties. In this particular series, $TbMnO_3$ exhibits low-temperature tunable magnetoelectric multiferroic behavior [6,7]. $TbFeO_3$ exhibits a commensurate spin order driven by Tb-Tb and Tb-Fe interactions [8] and has been reported to be a potentially promising dielectric material [9], along with $TbCrO_3$, showing similar properties [5]. Far less is known about $TbCoO_3$ and $TbNiO_3$, except for the existence of a low-temperature Tb-driven noncollinear magnetic order below 3.3 K in $TbCoO_3$ [10] and theoretically predicted magnetic ground states in $TbNiO_3$ [11].

The recent introduction of high-entropy oxide perovskites (HEOPs), both in the bulk [12–14] and thin film form [15,16], provides a new route towards the creation of novel designer ferroics. In high-entropy oxides or alloys, five or more elements are combined in equiatomic fashion to occupy the same lattice sites, resulting in high-quality single crystals [17,18]. The diversity of material designs based on entropy-driven phase stabilization enables the engineering of novel complex oxides with interesting properties, including enhanced wear-resistant coatings, thermoelectric properties, thermal insulation, catalysis, water splitting, and energy storage [17,18]. With respect to HEOPs, $La(Fe_{0.2}Mn_{0.2}Co_{0.2}Cr_{0.2}Ni_{0.2})O_3$ (L5BO) and its various stoichiometric variations have been the main focus of recent research [12,15,19,20]. Based on initial findings, L5BO features predominantly G-type antiferromagnetic order interspersed with ferromagnetic clusters [12,15]. This order competition is believed to be driven by Mn^{4+}, as B-O-B superexchange bonds containing Mn support ferromagnetic ordering, while most other bond combinations favor antiferromagnetic order [20].

In this Letter, we investigate how replacing La at the rare-earth sites with Tb affects the overall magnetic response and functional properties of HEOP thin films. We demonstrate the stabilization of HEOP $Tb(Fe_{0.2}Mn_{0.2}Co_{0.2}Cr_{0.2}Ni_{0.2})O_3$ (T5BO) single-crystal thin films. In addition to structural characterization, we performed element-sensitive measurements of emerging magnetism in T5BO using x-ray absorption spectroscopy (XAS) and x-ray magnetic circular dichroism (XMCD) spectroscopy at the $L_{2,3}$ absorption edges of all transition metal elements. Finally, the macroscopic magnetic response is compared to XMCD hysteresis loops, providing a strategy to distinguish how the different elements contribute to the magnetic properties.

Using pulsed laser deposition (PLD), we grew T5BO thin films on atomically flat TiO_2-terminated $SrTiO_3$ (STO) substrates with a (001) orientation. Thin film growth via PLD offers a variety of single-crystal stabilization mechanisms that go beyond the simple entropy-driven stabilization concept. These include substrate-induced stabilization mechanisms and growth parameters such as substrate temperature, pressure, and laser fluence. A KrF excimer laser ($\lambda = 248$ nm) operating at 5 Hz was used for target ablation, with a laser fluence of 1.4 J/cm^2 and a target-substrate distance of 5.5 cm. Optimal growth conditions were achieved when the substrate was held at a temperature of 840 °C, with an oxygen partial pressure of 0.12 mbar. A relatively slow growth rate was observed with 20 000 laser pulses resulting in 10-nm-thick films. Following the growth, the films were cooled down to 260 °C with a cooling rate of 4 °C/min under an oxygen pressure of 100 mbar.

*alan.farhan@gmx.net

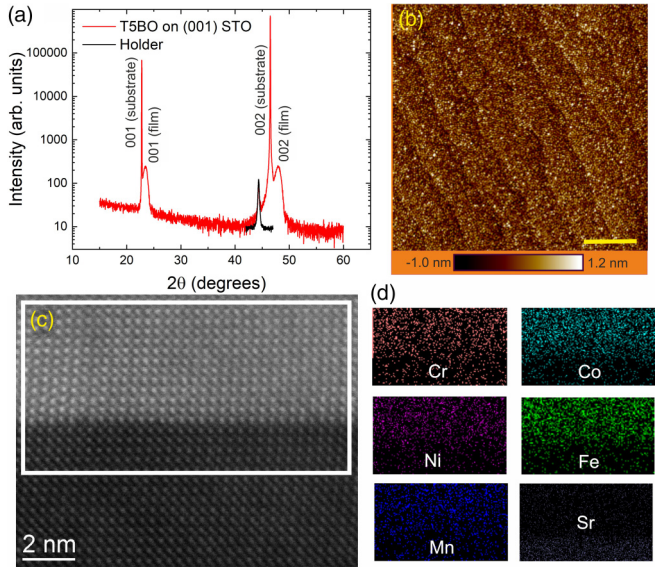

FIG. 1. (a) XRD scan of a 10-nm-thick T5BO film grown on a (001)-oriented STO substrate. (b) AFM image of the same film revealing a smooth surface with an average roughness of 0.523 nm. The terraces of the underlying TiO_2-terminated STO substrate are still visible. The yellow scale bar represents a length of 400 nm. (c) High-resolution STEM image of the same film taken along the [100] direction. (d) Element-sensitive EDX analysis showing a random and homogeneous distribution of transition metal elements throughout the T5BO thin film. The noisy EDX measurement points for some transition metal elements within the substrate area can be attributed to partial overlaps of absorption edges of these transition metals with Ti.

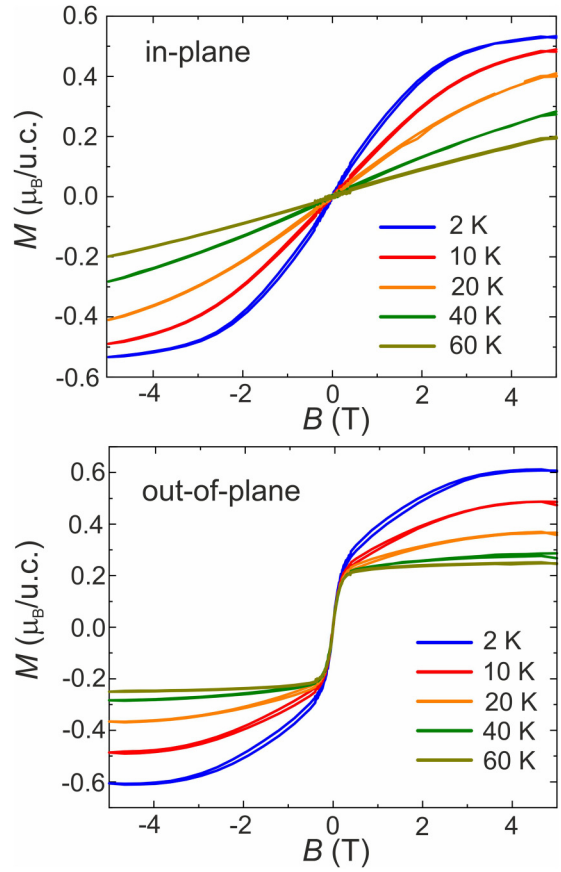

FIG. 2. Magnetic hysteresis loops of a 10-nm-thick T5BO film grown on a STO (001) substrate recorded at various temperatures, both with (a) in-plane and (b) out-of-plane magnetic fields. Due to a large out-of-plane anisotropy, the in-plane magnetization does not saturate for fields of up to 5 T.

As determined by the x-ray diffraction (XRD) scan shown in Fig. 1(a), the T5BO thin films are single crystalline with an out-of-plane lattice parameter $c = 3.761$ Å. Growth of T5BO onto STO (001) substrates ($a = 3.905$ Å) thus induces tensile film strain. Atomic force microscopy (AFM) was performed to determine the surface morphology [Fig. 1(b)]. The surface of the T5BO films is smooth with an average roughness of 0.523 nm and the terraces of the STO substrates are still visible. Scanning transmission electron microscopy (STEM) measurements demonstrate coherent epitaxial growth of T5BO films on STO (001) with an abrupt interface and a low density of structural defects [Fig. 1(c)]. We performed energy dispersive x-ray (EDX) spectroscopy [see Fig. 1(d)], revealing that the transition metal elements (Cr, Fe, Co, Ni, and Mn) are homogeneously distributed across the T5BO film and no signs of clustering of elements across the investigated region are measured.

Following this structural and chemical analysis, we now turn our focus to the magnetic properties of T5BO. Using a superconducting quantum interference device (SQUID) magnetometer from Quantum Design, we recorded magnetic hysteresis loops, with the magnetic field applied both parallel (in-plane) and vertically (out-of-plane) with respect to the film surface (see Fig. 2). Looking at the in-plane measurements as a function of temperature [Fig. 2(a)], we observe negligible magnetic hysteresis of the magnetization with a small opening and large saturation fields beyond 5 T. The out-of-plane magnetization curves [Fig. 2(b)] are shaped differently, with the measurement at 2 K showing a wasp-waisted hysteresis typical of complex multiphase ordering, similar to previous reports on L5BO bulk crystals and thin films [12,15]. The shape of the out-of-plane hysteresis curves changes with increasing temperature, resembling that of a soft magnet with small coercivity at 60 K [Fig. 2(b)]. The SQUID magnetometry data indicate ferromagnetic ordering with a significant strain-induced perpendicular magnetic anisotropy. This persistent soft magnetic response to out-of-plane applied fields stands in contrast to comparable L5BO thin films grown on (001) STO, where a significant hardening of the magnetization reversal is reported with increasing temperature [15]. A comparison of zero-field-cooled and field-cooled magnetization measurements (see SM 2 in the Supplemental Material [23]) indicates a transition temperature around 75 K.

Although SQUID measurements provide a macroscopic view of the overall magnetic response of the T5BO thin films, synchrotron-based XAS, employing x-ray magnetic circular dichroism (XMCD) [21], can pick the magnetic contributions apart on an element-by-element basis. This is done by recording x-ray absorption spectra around the L_2 and L_3 absorption edges of all five transition metal elements within the 5B-block using both circular right ($c+$) and circular left ($c-$)

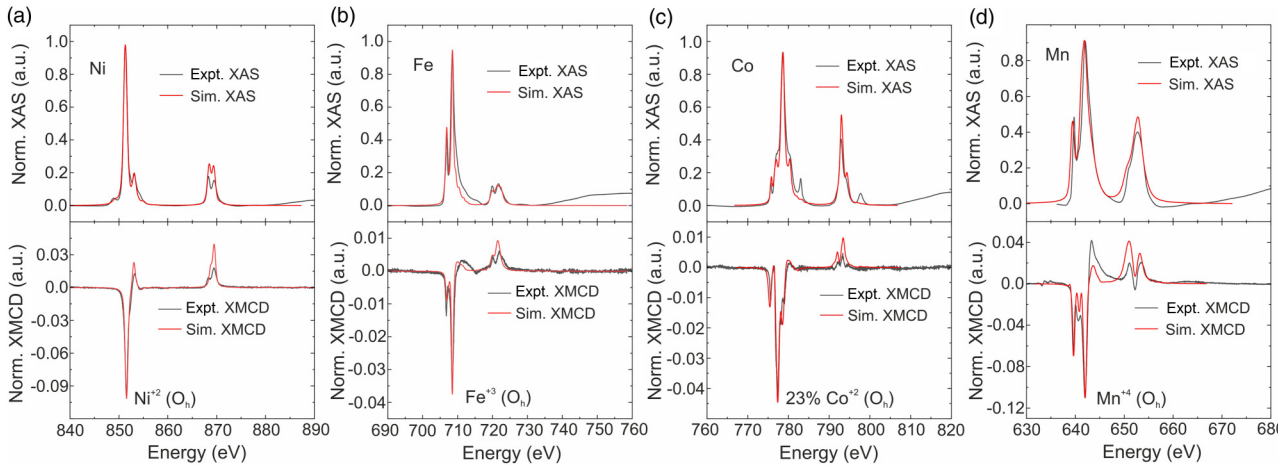

FIG. 3. X-ray absorption spectra (upper panels) and XMCD spectra (lower panels) around the $L_{2,3}$ absorption edges of (a) Ni, (b) Fe, (c) Co, and (d) Mn. Around the Co edges, close to 785 and 880 eV, we see the $M_{4,5}$ x-ray absorption near-edge spectrum (XANES) of Ba. This is due to a small (far less than 1%) Ba impurity in the PLD target. The small peak before the Ni rises from a La contamination, which is estimated to be below 0.2%. All measurements were performed with a magnetic field ($B = 6$ T) applied out of plane.

polarized x rays (Fig. 3, upper panels). The XAS measurements were performed by total electron yield (TEY) detection at the X-Treme beam line of the Swiss Light Source [22]. Subtracting $c+$ and $c-$ spectra from one another gives the normalized XMCD signal for all five transition elements (Fig. 3, lower panels, and the Supplemental Material [23]). These measurements were performed at 2.5 K in an out-of-plane geometry, where both the magnetic field (6 T) and x rays are perpendicular to the surface. Figure 3 compares the experimental XAS and XMCD spectra (black lines) and simulations performed with CTM4XAS [24] using multiplet ligand field theory (red lines). The computations are carried out by selecting the electric configuration of the element and by tuning the parameters, which are related to the crystal field splitting, used to account for the octahedral component, the spin orbit coupling and the screening and mixing effects, simulated by the reduction of the Slater integrals. The intrinsic broadening of each edge, associated to lifetime effects, is simulated by convoluting the calculated natural spectra with a Lorentzian [25]. To correctly fit the experimental data, a Gaussian broadening of 0.2 eV is used to account for the experimental broadening and the simulation is shifted by −2.1 eV in the photon energy. From the analysis of these spectra, the following picture emerges: The XAS and XMCD spectra for Ni [shown in Fig. 3(a)] indicate a dominant if not pure presence of octahedral Ni^{2+} [28,29], with a large magnetic moment. The Fe $L_{2,3}$ spectra [Fig. 3(b)] are consistent with a dominant presence of octahedral Fe^{3+} (O_h) and the absence of tetrahedral Fe^{3+} [26]. The Co XAS and XMCD spectra [see Fig. 3(c)], in contrast, reveal a mixture of high-spin Co^{2+} and low-spin Co^{3+}. For this element, the XMCD signal arises from the estimated 23% of octahedral Co^{2+} (O_h) [27], whereas the 77% low-spin Co^{3+} does not contribute to the XMCD signal. From the XAS and XMCD spectra of Mn [Fig. 3(d)], we derive a dominance of Mn^{4+} [30,31]. Similarly, the Cr spectra (see the Supplemental Material [23]) show a pure presence of octahedral Cr^{3+} [32]. From this mixture of valencies, we can already conclude ferromagnetism to emerge from X-O-Y superexchange interactions involving Mn^{4+}, for example $Mn^{4+} - O - Co^{2+}$, $Mn^{4+} - O - Ni^{2+}$, while most combinations involving Fe or Cr are expected to support antiferromagnetism [19].

The orbital (m_L), spin (m_S) and total magnetic moment ($m_L + m_S$) per average transition metal ion can be estimated by applying XMCD sum rules [33–35] to the recorded XAS and XMCD spectra. For $L_{2,3}$ XMCD spectra, the signal is directly proportional to the atomic magnetic moment of the excited transition metal ion. Using an approach where spin-quadruple contributions are neglected [36], we extracted the orbital (m_L) and spin (m_S) moments, in addition to the ratio (m_L/m_S). It should be noted that sum rules require a good separation between the L_2 and L_3 absorption edges, which for Ni, Co, and Fe is far better than for early transition metal elements such as Cr and Mn. For the latter elements, significant correction factors are needed [37]. Leaving Cr out for the aforementioned reasons, the results of these calculations are summarized in Table I. The most glaring results from this sum rule analysis are the large spin magnetic moment obtained for Mn ($m_S = -1.6\,\mu_B$), which is more than three times the spin magnetic moment of Fe ($m_S = -0.46\,\mu_B$). Furthermore, the ratio $m_L/m_S = 0.63$ for Co is significantly larger than for all the other elements, which can be attributed to distortions resulting from the tensile strain in the T5BO thin film [38].

To distinguish how the five transition metal elements contribute to the magnetization reversal process in the T5BO films, we recorded XMCD hysteresis loops [39] for all transition metal elements. In an out-of-plane geometry, we recorded XMCD hysteresis loops for magnetic fields between −6 T and +6 T with a step size of 0.1 T per measurement. The measurements were conducted at 2.5 and 50 K (Fig. 4). Interestingly, it is Ni that shows the largest opening in its hysteresis curve, which closes around 50 K. Mn, Co, and Fe show similar XMCD hysteresis loops, but with decreasing XMCD signal upon saturation. Finally, Cr features only a very weak hysteresis, which disappears around 50 K. These element-sensitive XMCD hysteresis loops, with their clear openings, differ from the macroscopic hysteresis loops shown in Fig. 2. This can be attributed to the fact that we probe a limited spot size (around

TABLE I. XMCD sum rule analysis for four transition metal ions in T5BO. Due to the large overlap of the L_2 and L_3 absorption edges in Cr and the inaccuracies that come with it, Cr was left out of the sum rule analysis.

Element (corr. factor)	No. holes	m_S (μ_B)	m_L (μ_B)	m_L/m_S
Ni (0.9)	2	−0.36(3)	−0.086(8)	0.23
Mn (0.59)	7	−1.6(1)	0.014(1)	−0.009
Co (0.89)	3	−0.13(1)	−0.082(8)	0.63
Fe (0.68)	5	−0.46(4)	−0.038(3)	0.08

160×160 μm^2) and depth of 4–6 nm with XMCD, while SQUID magnetometry measures the whole volume of film and substrate, including the interface between them.

In summary, we demonstrated the growth of high-quality single-crystal entropy-stabilized T5BO thin films, which feature a complex magnetic multiphase as a result of a large range of possible superexchange interactions between the transition metal elements within the 5B block. Combinations involving Mn^{4+} and high-spin Co^{2+} are likely drivers of the observed ferromagnetism in T5BO, which is embedded in an antiferromagnetic matrix. This type of multiphase ordering appears to be a common feature in HEOPs. Our element-sensitive study provides a route for further studies on how rare-earth ion choices and stoichiometric variations within the transition metal block affect the ionic configuration and interactions, with direct consequences on the overall ferroic properties. As an example, it remains an interesting open question on how the portion of high-spin Co^{2+} can be tuned by either rare-earth ion selection or strain-induced effects by growing T5BO thin films on various substrates.

The authors thank L. Flajšman, M. Valvidares, and P. Gargiani for their support and fruitful discussions. This work was supported by the Academy of Finland (Project No. 316857) and part of this work was performed at the XTreme beam line of the Swiss Light Source. F.S. is funded by the Swiss National Science Foundation (SNF) (Grant No. 200021_184684). SQUID-VSM measurements were carried out on the Quantum Design MPMS3-137 device of the Laboratory for Mesoscopic Systems, ETH Zurich, Switzerland and the Laboratory for Multiscale Materials Experiments, Paul Scherrer Institute, Switzerland. We acknowledge the provision of facilities and technical support by Aalto University at OtaNano - Nanomicroscopy Center (Aalto-NMC).

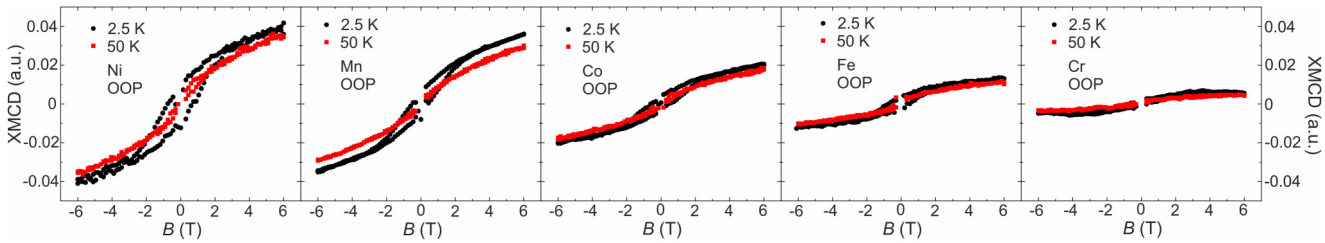

FIG. 4. XMCD hysteresis loops recorded at the L_3 edge of all five transition elements (Ni, Mn, Co, Fe, and Cr) involved in T5BO thin films. All measurements were performed with an out-of-plane magnetic field.

[1] M. Fiebig, T. Lottermoser, D. Meier, and M. Trassin, Nat. Rev. Mater. **1**, 16046 (2016).
[2] J. M. D. Coey, M. Viret, and S. von Molnar, Adv. Phys. **48**, 167 (1999).
[3] T. Kimura, T. Goto, H. Shintani, K. Ishizaka, T. Arima, and Y. Tokura, Nature (London) **426**, 55 (2003).
[4] Y. Tokunaga, S. Iguchi, T. Arima, and Y. Tokura, Phys. Rev. Lett. **101**, 097205 (2008).
[5] L. H. Yin, J. Yang, P. Tong, X. Luo, C. B. Park, K. W. Shin, W. H. Song, J. M. Dai, K. H. Kim, X. B. Zhua, and Y. P. Sun, J. Mater. Chem. C **4**, 11198 (2016).
[6] M. Matsubara, S. Manz, M. Mochizuki, T. Kubacka, A. Iyama, N. Aliouane, T. Kimura, S. L. Johnson, D. Meierand, and M. Fiebig, Science **348**, 1112 (2015).
[7] K. Shimamoto, S. Mukherjee, S. Manz, J. S. White, M. Trassin, M. Kenzelmann, L. Chapon, T. Lippert, M. Fiebig, C. W. Schneider, and C. Niedermayer, Sci. Rep. **7**, 44753 (2017).
[8] S. Artyukhin, M. Mostovoy, N. Paduraru Jensen, D. Le, K. Prokes, V. G. de Paula, H. N. Bordallo, A. Maljuk, S. Landsgesell, H. Ryll, B. Klemke, S. Paeckel, K. Kiefer, K. Lefmann, L. Theil Kuhn, and D. N. Argyriou, Nat. Mater. **11**, 694 (2012).
[9] P. Gupta, P. K. Mahapatra, and R. N. P. Choudhary, Phys. Status Solidi (b) **257**, 1900236 (2020).
[10] K. Knížek, Z. Jirák, P. Novák, and C. la Cruz, Solid State Sci. **28**, 26 (2014).
[11] L. Zhang, Y. Han, H. Khachai, R. Khenata, and X. Wang, J. Magn. Magn. Mater. **492**, 165645 (2019).
[12] R. Witte, A. Sarkar, R. Kruk, B. Eggert, R. A. Brand, H. Wende, and H. Hahn, Phys. Rev. Materials **3**, 034406 (2019).
[13] R. Witte, A. Sarkar, L. Velasco, R. Kruk, R. A. Brand, B. Eggert, K. Ollefs, E. Weschke, H. Wende, and H. Hahn, J. Appl. Phys. **127**, 185109 (2020).

[14] Y. Yin, F. Shi, G.-Q. Liu, X. Tan, J. Jiang, A. Tiwari, and B. Li, Appl. Phys. Lett. **120**, 082404 (2022).
[15] Y. Sharma, Q. Zheng, A. R. Mazza, E. Skoropata, T. Heitmann, Z. Gai, B. Musico, P. F. Miceli, B. C. Sales, V. Keppens, M. Brahlek, and T. Z. Ward, Phys. Rev. Materials **4**, 014404 (2020).
[16] Y. Sharma, B. L. Musico, X. Gao, C. Hua, A. F. May, A. Herklotz, A. Rastogi, D. Mandrus, J. Yan, H. N. Lee, M. F. Chisholm, V. Keppens, and T. Z. Ward, Phys. Rev. Materials **2**, 060404(R) (2018).
[17] R.-Z. Zhang and M. J. Reece, J. Mater. Chem. A **7**, 22148 (2019).
[18] E. P. George, D. Raabe, and R. O. Ritchie, Nat. Rev. Mater. **4**, 515 (2019).
[19] A. R. Mazza, E. Skoropata, Y. Sharma, J. Lapano, T. W. Heitmann, B. L. Musico, V. Keppens, Z. Gai, J. W. Freeland, T. R. Charlton, M. Brahlek, A. Moreo, E. Dagotto, and T. Z. Ward, Adv. Sci. **9**, 2200391 (2022).
[20] A. R. Mazza, E. Skoropata, J. Lapano, J. Zhang, Y. Sharma, B. L. Musico, V. Keppens, Z. Gai, M. J. Brahlek, A. Moreo, D. A. Gilbert, E. Dagotto, and T. Z. Ward, Phys. Rev. B **104**, 094204 (2021).
[21] Y. Wu, J. Stöhr, B. D. Hermsmeier, M. G. Samant, and D. Weller, Phys. Rev. Lett. **69**, 2307 (1992).
[22] C. Piamonteze, U. Flechsig, S. Rusponi, J. Dreiser, J. Heidler, M. Schmidt, R. Wetter, M. Calvi, T. Schmidt, H. Pruchova, J. Krempasky, C. Quitmann, H. Brune, and F. Nolting, J. Synchrotron Radiat. **19**, 661 (2012).
[23] See Supplemental Material at http://link.aps.org/supplemental/10.1103/PhysRevB.106.L060404 for XAS and XMCD spectra around the Cr $L_{2,3}$ edges and temperature-dependent magnetometry on T5BO.
[24] E. Stavitski and F. M. F. de Groot, Micron **41**, 687 (2010).
[25] M. O. Krause and J. H. Oliver, J. Phys. Chem. Ref. Data **8**, 329 (1979).
[26] R. V. Chopdekar, M. Liberati, Y. Takamura, L. F. Kourkoutis, J. S. Bettinger, B. B. Nelson-Cheeseman, E. Arenholz, A. Doran, A. Scholl, D. A. Muller, and Y. Suzuki, J. Magn. Magn. Mater. **322**, 2915 (2010).
[27] C. Moya, A. Fraile Rodríguez, M. Escoda-Torroella, M. García del Muro, S. R. V. Avula, C. Piamonteze, X. Batlle, and A. Labarta, J. Phys. Chem. C **125**, 691 (2021).
[28] J. Lumetzberger, M. Buchner, S. Pile, V. Ney, W. Gaderbauer, N. Daffé, M. V. Moro, D. Primetzhofer, K. Lenz, and A. Ney, Phys. Rev. B **102**, 054402 (2020).
[29] C. Klewe, M. Meinert, A. Boehnke, K. Kuepper, E. Arenholz, A. Gupta, J.-M. Schmalhorst, T. Kuschel, and G. Reiss, J. Appl. Phys. **115**, 123903 (2014).
[30] J.-S. Kang, S. M. Lee, D. H. Kim, S. Kolesnik, B. Dabrowski, B.-G. Park, J.-Y. Kim, J. Lee, B. Kim, and B. I. Min, J. Appl. Phys. **107**, 09D721 (2010).
[31] C. Mitra, Z. Hu, P. Raychaudhuri, S. Wirth, S. I. Csiszar, H. H. Hsieh, H.-J. Lin, C. T. Chen, and L. H. Tjeng, Phys. Rev. B **67**, 092404 (2003).
[32] G. Vinai, A. Khare, D. S. Rana, E. Di Gennaro, B. Gobaut, R. Moroni, A. Yu. Petrov, U. Scotti di Uccio, G. Rossi, F. Miletto Granozio, G. Panaccione, and P. Torelli, APL Mater. **3**, 116107 (2015).
[33] B. T. Thole, P. Carra, F. Sette, and G. van der Laan, Phys. Rev. Lett. **68**, 1943 (1992).
[34] P. Carra, B. T. Thole, M. Altarelli, and X. Wang, Phys. Rev. Lett. **70**, 694 (1993).
[35] C. T. Chen, Y. U. Idzerda, H.-J. Lin, N. V. Smith, G. Meigs, E. Chaban, G. H. Ho, E. Pellegrin, and F. Sette, Phys. Rev. Lett. **75**, 152 (1995).
[36] C. Piamonteze, P. Miedema, and F. M. F. de Groot, Phys. Rev. B **80**, 184410 (2009).
[37] Y. Teramura, A. Tanaka, and T. Jo, J. Phys. Soc. Jpn. **65**, 1053 (1996).
[38] L. López-Mir, R. Galceran, J. Herrero-Martín, B. Bozzo, J. Cisneros-Fernández, E. V. Pannunzio Miner, A. Pomar, L. Balcells, B. Martínez, and C. Frontera, Phys. Rev. B **95**, 224434 (2017).
[39] B. B. Nelson-Cheeseman, R. V. Chopdekar, J. S. Bettinger, E. Arenholz, and Y. Suzuki, J. Appl. Phys. **103**, 07B524 (2008).